



Nanoscale

**Adsorption of Ethylenediamine on Cu Surfaces: Attributes of  
a Successful Capping Molecule Using First-Principles  
Calculations**

Journal:	<i>Nanoscale</i>
Manuscript ID	NR-ART-05-2021-003173.R1
Article Type:	Paper
Date Submitted by the Author:	08-Jul-2021
Complete List of Authors:	Chen, Zihao; The Pennsylvania State University University Park, Chemical Engineering Fichthorn, Kristen; Pennsylvania State University,

SCHOLARONE™  
Manuscripts

## ARTICLE

# Adsorption of Ethylenediamine on Cu Surfaces: Attributes of a Successful Capping Molecule Using First-Principles Calculations

Zihao Chen<sup>a</sup> and Kristen A. Fichthorn<sup>a,b\*</sup>Received 00th January 20xx,  
Accepted 00th January 20xx

DOI: 10.1039/x0xx00000x

The shape-controlled synthesis of Cu nanocrystals can benefit a wide range of applications, though challenges exist in achieving high and selective yields to a particular shape. Capping agents play a pivotal role in controlling shape, but their exact role remains ambiguous. In this study, the adsorption of ethylenediamine (EDA) on Cu(100) and Cu(111) was investigated with quantum density functional theory (DFT) to reveal the complex roles of EDA in promoting penta-twinned Cu nanowire growth. We find EDA has stronger binding on Cu(100) than on Cu(111), which agrees the general expectation that penta-twinned Cu nanowires express facets with stronger capping-molecule binding. Despite this stronger binding, *ab initio* thermodynamics reveals the surface energy of EDA-covered Cu(111) is lower than that EDA-covered Cu(100) at all solution-phase EDA chemical potentials. We also investigated the capability of EDA to protect Cu surfaces from oxidation in water by quantifying energy barriers for a water molecule to diffuse through EDA layers on Cu(100) and Cu(111). The energy barrier on Cu(100) is significantly lower, which supports observations of faster oxidation of Cu(100) in electrochemical experiments. Thus, we elucidate another possible function of a capping agent – to enable selective oxidation of crystal facets. This finding adds to the general understanding of successful attributes of capping agents for shape-selective nanocrystal growth.

## Introduction

Metal nanocrystals have attracted significant attention for their capability to advance a variety of cutting-edge applications, including selective catalysis,<sup>1–4</sup> energy storage,<sup>5,6</sup> electronic devices,<sup>7–12</sup> and fuel cells.<sup>13,14</sup> While it is evident that the beneficial properties of nanocrystals for these applications depend sensitively on their size and shape, achieving high and selective yields of various nanocrystal morphologies remains a challenge. In solution-phase syntheses, which are particularly effective and widely applied for metal nanocrystals, capping agents are important for achieving shape control.<sup>15</sup> For example, the shape-selective growth of Ag nanocrystals has been linked to capping molecules such as polyvinylpyrrolidone (PVP) and citric acid,<sup>16–19</sup> while the formation of Cu nanowires is often attributed to linear alkylamines.<sup>20–23</sup>

Many studies have postulated that capping agents affect crystal structure by adsorbing selectively to facets that constitute the majority in the crystal shape.<sup>20,21,24–27</sup> While this hypothesis has been corroborated by quantum density-functional theory (DFT) studies for several different systems,<sup>28–36</sup> it is evident that binding selectivity provides a limited picture of how capping molecules actuate shape control. Capping agents can function in a number of ways, by influencing the kinetics of crystal growth,<sup>37–39</sup> or the thermodynamics of crystal shape.<sup>40–43</sup> Recent studies show there can

be a complex synergy between capping agents and other solution-phase additives that dictates nanocrystal shape.<sup>43–45</sup> In the growth of penta-twinned Cu nanowires, for example, it was recently demonstrated that solution-phase chloride from the CuCl<sub>2</sub> precursor can selectively disrupt the adsorption of hexadecylamine (HDA) capping agent from Cu(111), but not from Cu(100). In this way, the {111} facets are open to Cu addition but the {100} facets are blocked, facilitating growth of the nanowires. Another complex synergy has been suggested for the ethylenediamine (EDA)-mediated growth of penta-twinned Cu nanowires, in which EDA was experimentally observed to prevent the oxidation of Cu(111), while allowing for the oxidation of Cu(100). This phenomenon increased the reduction rate of the Cu(OH)<sub>2</sub><sup>–</sup> ion (and the Cu deposition rate) on Cu(111) relative to Cu(100), enhancing the growth of long wires.<sup>20,46</sup> In the work discussed below, we present an investigation of this experimental finding using dispersion-corrected DFT.

## Methods

To elucidate the role of EDA in Cu nanowire growth, we studied its adsorption on Cu(100) and Cu(111) using dispersion-corrected DFT. Although DFT calculations probe a zero-temperature environment far removed from the liquid-phase conditions in experiment, DFT calculations of adsorption in vacuum can nevertheless reveal trends of the surfaces that occur in liquid-phase systems at finite temperatures.<sup>29,31,45,47–52</sup> Periodic DFT calculations were performed using the Vienna Ab initio Simulation Package (VASP),<sup>53–55</sup> with the projector-augmented wave method.<sup>56,57</sup> All calculations used the generalized gradient approximation with the exchange-correlation functional by Perdew, Burke, and Ernzerhof.<sup>58</sup> The energy cut-off for the plane-wave basis set was set to 450 eV. Structural optimization was performed with a convergence criterion of 10<sup>–6</sup> eV on the electronic self-consistent energy and 0.01 eV/Å on

<sup>a</sup> Department of Chemical Engineering, The Pennsylvania State University, University Park, PA 16802

<sup>b</sup> Department of Physics, The Pennsylvania State University, University Park, PA 16802.

\*fichthorn@psu.edu

Electronic Supplementary Information (ESI) available: [details of any supplementary information available should be included here]. See DOI: 10.1039/x0xx00000x

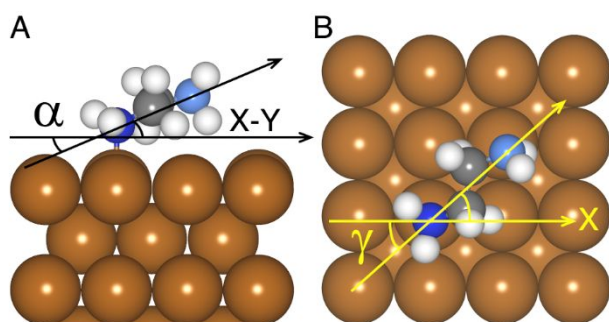


**Figure 1.** Side view (A) and top-down view (B) of the EDA adsorption model used in this study. The angles  $\alpha$  and  $\gamma$  are explained in the text. (Brown: Cu, Dark Blue: bound N, Light Blue: unbound N, Gray: C, and White: H).

the forces for all calculations. Monkhorst-Pack grids were used for integration over the first Brillouin zone with a Methfessel–Paxton smearing of 0.1 eV.<sup>59</sup> To account for long-range van der Waals (vdW) interactions, we used the DFT-D2 method.<sup>60</sup> We used the parameters for Cu suggested by Ruiz *et al.*<sup>61</sup> to account for screening effects in the bulk metal and used the parameters from Grimme for all other species. By using DFT-D2 with the parameters by Ruiz *et al.*,<sup>61</sup> we limit over-estimation of the vdW interaction. The cut-off radius for vdW interactions was 40.0 Å.

We used a periodic unit cell to model the adsorption of all-*trans* EDA, which consists of a Cu surface with molecules adsorbed on the top layer as shown in **Figure 1**. We adopted a vacuum spacing of about 38 Å in the direction normal to the surface to minimize interactions between periodic images. The Cu surfaces were modelled as six-layer slabs. During optimization, the top three Cu layers and the adsorbed molecules were allowed to fully relax, while the bottom three Cu layers were fixed at bulk positions using the experimental lattice constant of 3.615 Å.<sup>62</sup> A dipole correction was introduced along the surface normal direction to prevent interaction between periodic images in this asymmetric system.

We used several different geometric measures to characterize EDA adsorption. One measure is the average bond distance  $d_{\text{Cu}-\text{N}}$  between an N atom and the closest Cu atom in the surface. Because EDA contains two N atoms, we calculated two distances:  $d_{\text{N}-\text{Cu}}^1$  and  $d_{\text{N}-\text{Cu}}^2$ . We also characterized the tilt and orientation angles of the adsorbed molecules. The tilt angle  $\alpha$  is defined as the angle between the chain axis that connects two N atoms of EDA and the  $x$ - $y$  plane parallel to the surface, while the orientation angle  $\gamma$  is defined as the angle between the  $x$ -axis and the surface projection of the chain axis, as depicted in **Figure 1**.

We studied the binding of EDA on Cu(100) and Cu(111) at different coverages, ranging from 0.08 to 0.25 monolayer (ML), where coverage is defined as the ratio of the number of adsorbed EDA to the number of Cu atoms in the top layer of the slab. At the highest coverage studied – 0.25 ML, a  $(9 \times 9 \times 1)$   $k$ -point mesh was used for the  $(2 \times 2)$  unit cell of Cu(100) and a  $(10 \times 6 \times 1)$  mesh was used for the  $(2 \times 2)$  unit cell of Cu(111). A  $(15 \times 15 \times 1)$   $k$ -point mesh was used for the bulk Cu calculation. For optimization of a single gas-phase molecule, we used a cubic unit cell with a side length

of 25.0 Å and a single  $k$ -point. **Table S1** in the Electronic Supplementary Information (ESI) contains details about the unit cells used for different coverages, along with the corresponding  $k$ -point meshes. **Table S2** summarizes the results of convergence tests for the calculations.

We used several different measures to characterize the energetics of EDA adsorption on the Cu surfaces. First, the binding energy  $E_{\text{bind}}$  is given by

$$E_{\text{bind}} = (N_{\text{EDA}}E_{\text{EDA}} + E_{\text{Cu}} - E_{\text{Cu-EDA}})/N_{\text{EDA}} \quad (1)$$

where  $E_{\text{EDA}}$  is the energy of an optimized EDA molecule in the gas phase,  $N_{\text{EDA}}$  is the number of EDA molecules in the unit cell,  $E_{\text{Cu}}$  is the energy of the bare, optimized Cu slab, and  $E_{\text{Cu-EDA}}$  is the total energy of the entire optimized adsorption system. We can then write the total binding energy as the sum of three types of interactions, such that

$$E_{\text{bind}} = E_{\text{EDA-EDA}} + E_{\text{EDA-Cu}} + \Delta E_{\text{Cu}} \quad (2)$$

The quantity  $E_{\text{EDA-EDA}}$  is a measure of through-space interactions between adsorbed capping molecules and is given by

$$E_{\text{EDA-EDA}} = (N_{\text{EDA}}E_{\text{EDA}} - E_{\text{EDA,o}})/N_{\text{EDA}} \quad (3)$$

where  $E_{\text{EDA,o}}$  is the energy of an isolated layer of capping molecules with the same configuration as in the optimized adsorption system, but in the absence of the Cu slab.  $E_{\text{EDA-EDA}}$  contains contributions from both intra- and inter-molecular interactions.

We also obtain  $E_{\text{EDA-Cu}}$ , which measures the interaction between an adsorbed molecule and the Cu slab, from

$$E_{\text{EDA-Cu}} = (E_{\text{EDA,o}} + E_{\text{Cu,o}} - E_{\text{Cu-EDA}})/N_{\text{EDA}} \quad (4)$$

Here  $E_{\text{Cu,o}}$  is the energy of a fixed Cu slab without adsorbed molecules but with the same configuration as in the optimized adsorption system. Similarly, the energy change in the Cu slab after binding  $\Delta E_{\text{Cu}}$  is given by

$$\Delta E_{\text{Cu}} = (E_{\text{Cu,o}} - E_{\text{Cu}})/N_{\text{EDA}} \quad (5)$$

The energetic quantities in Equations (1) – (5) can be partitioned into two different components: the vdW interaction and the short-range interaction. The short-range component of  $E_{\text{EDA-Cu}}$  can be seen as the strength of the chemical bond between adsorbed EDA and the Cu surface.

## Results and Discussion

**Table 1.** Geometric and energetic characteristics of optimal patterns for EDA adsorption on Cu(100) at various coverages  $\theta$ .

$\theta$ (ML)	$E_{\text{bind}}$ (eV)	$d_{\text{N}-\text{Cu}}^1$ (Å)	$d_{\text{N}-\text{Cu}}^2$ (Å)	$\alpha$ (°)	$\gamma$ (°)
0.25	1.00	2.14	3.38	16.2	41.6
0.17	1.01	2.12	3.59	15.3	72.8
0.13	1.03	2.10	3.61	21.0	42.5
0.08	1.06	2.10	3.54	14.6	74.5

A recent study using both molecular dynamics simulation and atomic force microscopy revealed linear alkylamines with six or less carbon atoms in the chain cannot form a stable self-assembled monolayer on graphene.<sup>63</sup> Similar results were found for linear alkylamines adsorbed on Cu surfaces.<sup>30</sup> Based on these observations for short-chain alkylamines, we adopted initial configurations in which EDA adsorbs flat, with its backbone parallel to the Cu surfaces. We initially considered all-*trans* EDA, which is more favored energetically than alternative *gauche* and eclipsed EDA structures. The initial distance between EDA and the Cu surface was set to 2.0 Å, which is close to the typical bond length of N-Cu, with a tilt angle of  $\alpha = 0^\circ$  as well as an orientation angle of  $\gamma = 0^\circ$  or  $45^\circ$  on Cu(100) and  $0^\circ$  or  $30^\circ$  on Cu(111). Different adsorption sites for the N in EDA including atop, bridge, and hollow sites were examined for both Cu(100) and Cu(111). By considering various sites for the N atom, as well as different tilt and orientation angles, we also place the C and H atoms at various initial positions with respect to the Cu surface atoms.

### EDA Binding on Cu(100)

**Table 1** summarizes the optimal EDA binding energies and configurations for the various coverages  $\theta$  probed on Cu(100). One notable feature of all the optimal binding configurations in **Table 1** is the nitrogen atom closest to a Cu surface atom always resides on top of a Cu atom, with  $d_{\text{N}-\text{Cu}}^1$  around 2.1 Å. Although we did consider various initial locations for the N atoms, the chemisorbed N atoms moved on top of Cu surface atoms during optimization in all cases. This is consistent with previous DFT studies of alkylamines on coinage metal surfaces.<sup>30,64</sup> We also find EDA essentially retains its optimal gas-phase configuration with regard to the torsion angle of the amine groups around the central C-C bond, and is slightly tilted, with  $\alpha$  between  $14^\circ$  and  $21^\circ$ .

**Figure 2A** shows the optimal binding conformation of EDA at the highest coverage of 0.25 ML. In this configuration, EDA is adsorbed on Cu(100) with a relatively small tilt angle of  $\alpha = 16^\circ$  and both N atoms are located above Cu surface atoms. We note the orientation angles for 0.25 and 0.13 ML coverages are both around  $\gamma = 45^\circ$ , while the orientation angles are relatively larger, at around  $75^\circ$  for 0.17 and 0.08 ML, such that the unbound N atom ( $x = 2$  in **Table 1**) resides above a fourfold hollow site instead of a top site. This likely results from steric interactions between nearest-neighbor EDA molecules, such that the unbound N atom prefers to reside above the fourfold hollow site if it is free, while the atop sites will be chosen when the hollow site is blocked by neighboring EDA molecules (see **Figure 2A**).

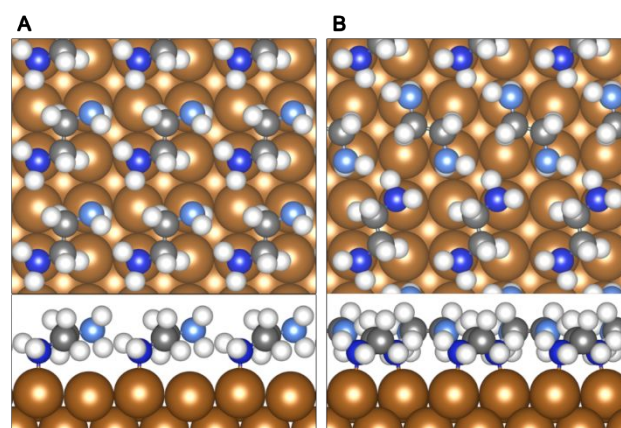


**Figure 2.** Top-down view (upper) and side view (lower) of EDA binding conformations on Cu(100) at 0.25 ML with the optimal pattern (A) and a higher-energy zig-zag pattern (B) (Brown: Cu, Dark Blue: bound N, Light Blue: unbound N, Gray: C, and White: H).

As discussed above, we can decompose the total binding energies listed in **Table 1** into three components [cf., Equation (2)] and we can decompose each component into short-range and vdW interactions. The values of these various energies are reported in **Table S3** and plotted in **Figure 3**. Here, we see the total binding energy per EDA molecule on Cu(100) increases slightly with decreasing coverage. The EDA-Cu interaction given by Equation (4) dominates the total binding energy, while the EDA-EDA interaction [Equation (3)] plays a minor role and  $\Delta E_{\text{Cu}}$  in Equation (5) (not shown) is negligible. Both vdW and short-range interactions contribute significantly to the total binding energy.

The short-range EDA-EDA interaction is negative for all cases due to structural distortions of EDA upon adsorption, while the vdW component of the EDA-EDA interaction is positive and increases with increasing coverage. Overall, a denser EDA adlayer has stronger vdW interactions between molecules at the expense of molecular distortion. The Cu slab is essentially unaltered upon adsorption and only Cu atoms bound to the N relax slightly outward from the Cu surface, leading to a negligible value for  $\Delta E_{\text{Cu}}$ .

**Figure 2B** shows another, less energetically favored zig-zag pattern for 0.25 ML. In this configuration, there is a mixture of chemically and physically adsorbed EDA molecules on Cu(100), such that half the EDA molecules chemisorb with both N atoms bound to atop sites and the other half “pop up” and reside away from the surface. Although the average binding energy of the zig-zag pattern in **Figure 2B** is only slightly lower than that in **Figure 2A**, the weakly physisorbed EDA molecules are susceptible to desorption into the solution phase and the surface would be less protected from oxidation.

### EDA Binding on Cu(111)

Geometric and energetic aspects of EDA adsorption on Cu(111) are summarized in **Table 2**. Similar to Cu(100), EDA binds to Cu(111)

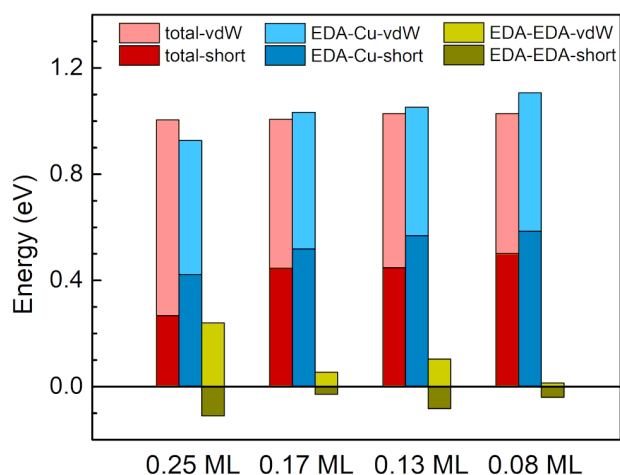


**Figure 3.** The total binding energy along with its decomposition into the EDA-Cu interaction and EDA-EDA interaction, each consisting of short-range and vdW components, for different coverages on Cu(100) listed in **Table 1**.

with one of the N atoms chemisorbed directly above a Cu surface atom and the other N is not bound. Although we did consider various initial locations for the N atoms, the chemisorbed N atoms moved on top of Cu surface atoms during optimization in all cases. The Cu-N bond length decreases with decreasing coverage and EDA essentially retains its gas-phase structure when it adsorbs, as we saw on Cu(100). Tilt angles are in general larger than those on Cu(100) at the same coverage – especially at the highest coverage of 0.25 ML – due to the denser packing of Cu atoms on the (111) surface, which leads to a denser packing of the EDA adlayer.

The optimal binding conformation at 0.25 ML is shown in **Figure 4A**. From the side view, as well as from **Table 2**, we see the tilt angle for this configuration is significantly larger than all other cases studied on both Cu(100) and Cu(111). Again, this derives from the high packing density of EDA, which is the highest density of EDA per area in all the stable patterns. We also tested the  $(\sqrt{3} \times \sqrt{3})R30^\circ$  unit cell on Cu(111) with 0.33 ML coverage, but the EDA density was too high and this configuration was unstable.

A decomposition of the total binding energy into its various components is shown in **Figure 5** and details can be found in **Table S3**. The EDA-Cu interaction dominates the total binding energy, as we saw for Cu(100), and this interaction increases

**Table 2.** Geometric and energetic characteristics of optimal patterns for EDA adsorption on Cu(111) at different coverages.  $d_{N-Cu}^x$  is the distance between N atom  $x$  and the nearest Cu atom.

$\theta$ (ML)	$E_{bind}$ (eV)	$d_{N-Cu}^1$ (Å)	$d_{N-Cu}^2$ (Å)	$\alpha$ (°)	$\gamma$ (°)
0.25	0.82	2.17	4.60	36.2	15.5
0.17	0.92	2.15	3.65	16.9	12.4
0.13	0.88	2.14	3.78	20.7	10.3
0.08	0.89	2.11	3.72	20.3	27.0

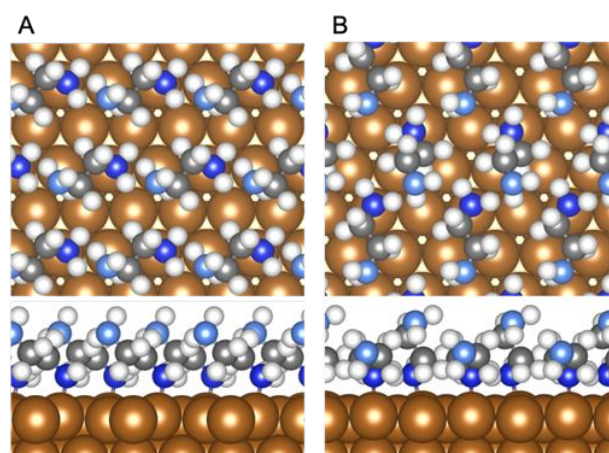


**Figure 4.** Top-down view (upper) and side view (lower) of EDA binding conformations on Cu(111) at 0.25 ML coverages with the lowest-energy arrangement (A) and a higher energy zig-zag arrangement (B) (Brown: Cu, Dark Blue: bound N, Light Blue: unbound N, Gray: C, and White: H).

with decreasing coverage. As for Cu(100), the EDA-Cu interaction correlates with the change in bond length, indicating shorter bonds are stronger for these systems. The overall EDA-EDA interaction increases with increasing coverage and the contribution from this component at 0.25 ML is notably large (0.22 eV), as EDA tilts away from the surface to achieve the optimal conformation. One notable difference between EDA adsorption on Cu(111) and Cu(100) is the overall binding energy exhibits a maximum at an intermediate coverage of 0.17 ML on Cu(111). This is a result of the balance between the EDA-Cu interaction, which decreases with increasing coverage, and the EDA-EDA interaction, which increases with increasing coverage. Overall, the total EDA binding energies on Cu(111) are less than the lowest binding energy on Cu(100).

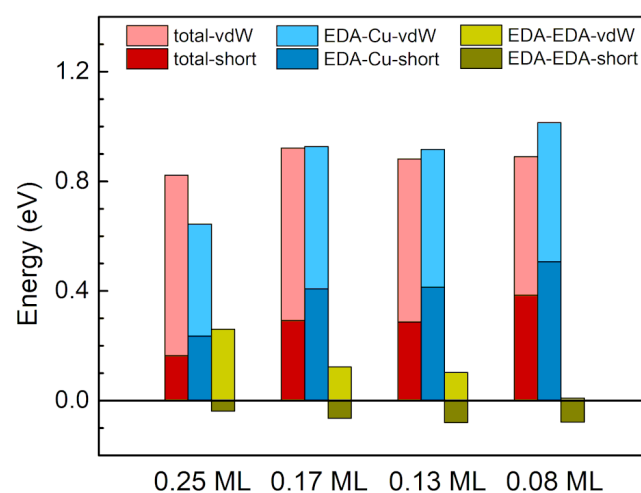


**Figure 5.** The total binding energy along with its decomposition into the EDA-Cu interaction and EDA-EDA interaction, each consisting of short-range and vdW components, for different coverages on Cu(100) listed in **Table 2**.

We also tested EDA adsorption in a zig-zag pattern on Cu(111) at 0.25 ML coverage, with the optimal conformation shown in **Figure 4B**. Unlike the EDA zig-zag pattern on Cu(100), all EDA molecules are adsorbed with one N bound at an atop site. The overall binding energy per EDA molecule in the zig-zag pattern is slightly weaker than the most stable pattern due to stronger structural distortions of adsorbed EDA. Thus, analysis of the binding of EDA to Cu(100) and Cu(111) shows stronger binding of EDA on Cu(100). The binding of EDA is influenced by the N-Cu bond strength, structural distortions in EDA, and through-space EDA-EDA interactions, in which the geometries of both EDA and the Cu surfaces play an important role.

### EDA-Mediated Cu Surface Energies

Capping molecules can affect both the thermodynamics and kinetics of nanocrystal growth. From the above studies, we see EDA binds stronger to Cu(100) than to Cu(111). This {100} binding preference opens the possibility for EDA adsorption to lower the surface energy of Cu(100) below that of Cu(111) and provide a thermodynamic driving force for {100} facet formation – the major facet in penta-twinned Cu nanowires. To assess this possibility, we performed *ab initio* thermodynamics calculations to identify the surface energies and EDA coverages of Cu(100) and Cu(111) facets for a fixed, solution-phase EDA chemical potential.

The surface energy of a Cu slab with adsorbed EDA is calculated using

$$\gamma_{\text{Cu-EDA}} = \frac{E_{\text{Cu-EDA}} - N_{\text{Cu}}E_{\text{Cu}}^{\text{bulk}} - N_{\text{EDA}}\mu_{\text{EDA}}}{A_{\text{surf}}} - \gamma_{\text{Cu}}^{\text{fixed}} \quad (6)$$

Here,  $N_{\text{Cu}}$  and  $E_{\text{Cu}}^{\text{bulk}}$  represent the number of Cu atoms in the unit cell and the energy of a bulk Cu atom, respectively,  $\mu_{\text{EDA}}$  is the chemical potential of EDA and  $A_{\text{surf}}$  is the surface area of the slab. The surface energy of the fixed side of the slab is given by

$$\gamma_{\text{Cu}}^{\text{fixed}} = \frac{E_{\text{slab, fixed}} - N_{\text{Cu}}E_{\text{Cu}}^{\text{bulk}}}{2A_{\text{surf}}} \quad (7)$$

Here  $E_{\text{slab, fixed}}$  is the energy of a Cu slab with atoms fixed at the bulk positions. For plotting purposes, we use  $\Delta\mu_{\text{EDA}}$ , which is given by  $\Delta\mu_{\text{EDA}} = (N_{\text{EDA}}\mu_{\text{EDA}} - E_{\text{EDA},0})/N_{\text{EDA}}$ .

**Figure 6** shows the surface energies of Cu(100) and Cu(111) as a function of  $\Delta\mu_{\text{EDA}}$  for all the EDA surface coverages probed in this study. Here, we see the lowest surface energy of Cu(111) for a fixed  $\Delta\mu_{\text{EDA}}$  is always lower than that of Cu(100). Thus, even though EDA binds more strongly to Cu(100) than to Cu(111), this stronger binding is not sufficient to overcome the lower energy of the bare Cu(111) surface. **Figure 6** shows EDA binding does lower the energies of both Cu(100) and Cu(111), but it does not reverse the trend seen for the bare surfaces and it does not provide a thermodynamic driving force for nanowire growth.

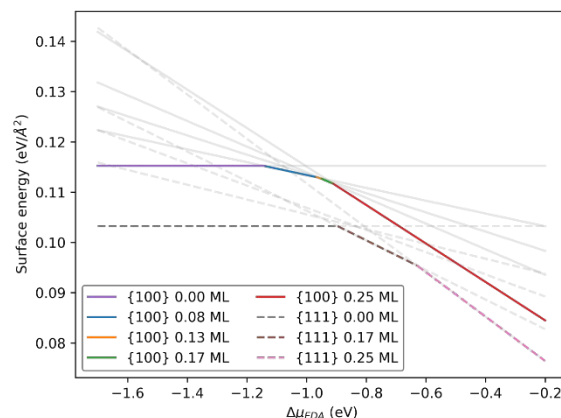


**Figure 6.** Surface energies of Cu(100) and Cu(111) as a function of the EDA chemical potential. The gray lines represent the results of all calculations, while the colored portions indicate the lowest surface energies for a given range of  $\Delta\mu_{\text{EDA}}$ .

### Electronic Structure of EDA on Cu

To gain further insight into the adsorption of EDA, we performed a charge density-difference analysis and we calculated the projected density of states (PDOS) upon adsorption. The charge density difference in EDA adsorption is given by

$$\Delta\rho = \rho_{\text{Cu-EDA}} - \rho_{\text{EDA}} - \rho_{\text{Cu}} \quad (8)$$

where  $\rho_{\text{Cu-EDA}}$  is the charge density of the entire optimized adsorption system,  $\rho_{\text{EDA}}$  is the density for an isolated EDA adlayer with the same configuration as in the optimized system but in the absence of the surface slab, and  $\rho_{\text{Cu}}$  represents the charge density of the bare Cu slab with the same configuration as in the optimized Cu-EDA system.

The case of adsorbed EDA on Cu(100) for the lowest-energy configuration at 0.25 ML is shown in **Figure 7A** using the Visualization for Electronic and Structural Analysis (VESTA)<sup>65</sup> software. We note on Cu(100), the most significant charge transfer takes place between the bound N atom in EDA and the Cu surface atom bound to the N. Charge is depleted from the Cu surface atoms and accumulates around the N atom. Additionally, there is minor charge redistribution around other C and N atoms in EDA, which is probably due to slight distortion of the molecular structure upon adsorption. Similar behavior is observed on Cu(111). The calculated charge transfer agrees well with a recent solution-phase NMR study showing that binding of amines on Cu origins from sharing the doublets in amine groups of alkylamines.<sup>66</sup> We note in ref. 30, the opposite conclusion was reached – namely that charge is transferred from the N to the Cu surface. This conclusion was due to the use of a lower iso-surface level, which failed to achieve complete spatial resolution of the charge transfer.

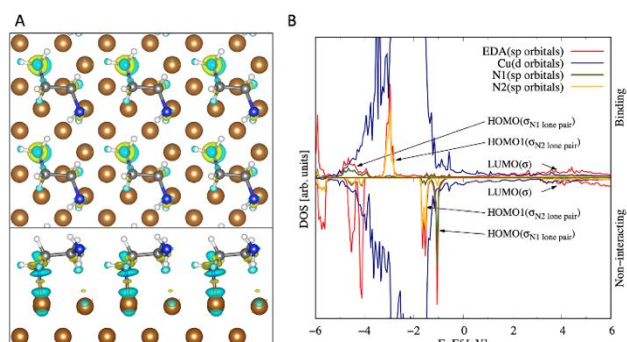


**Figure 7.** (A) Top-down view (upper) and side view (lower) of the charge-density difference in the lowest-energy configuration of EDA on Cu(100) at 0.25 ML coverage (Brown: Cu, Blue: N, Gray: C, White: H, Yellow: charge accumulation, Light blue: charge depletion). The sizes of atoms are scaled to show the charge distributions and an iso-surface level of  $\pm 0.0036$  Bohr<sup>-3</sup> is used. (B) PDOS analysis of EDA on Cu(100) with the same configuration as in (A). The Fermi energy is set to zero.

**Figure 7B** shows the PDOS of EDA on Cu(100) with the same configuration used for the charge density-difference analysis. **Figure 7B** includes a non-interacting configuration introduced by separating adsorbed EDA and the Cu(100) slab by  $\sim 16$  Å with their adsorption configurations intact. The frontier orbitals of interest include the highest occupied molecular orbital (HOMO) and HOMO-1, as well as the lowest unoccupied molecular orbital (LUMO). In the non-interacting limit, two peaks occur below the Fermi level, around -1.0 and -1.7 eV. These two peaks show that HOMO and HOMO-1 represent the lone-pair electrons of the two N atoms, with HOMO and HOMO-1 representing the bound and unbound N atoms, respectively. The difference in energy levels for the two N atoms occurs because of the asymmetric EDA structure induced by adsorption.

The most significant change in the PDOS from the non-interacting limit to the binding scenario in **Figure 7B** is a down-shift in the energy levels of the occupied orbitals. The HOMO is pushed much lower in energy (about 2.5 eV to the left) with broadened peaks compared to other orbitals and has significant overlap with the Cu *d* bands. This indicates the strong hybridization of the HOMO with the Cu *d* bands in the binding process, resulting in a delocalized peak with mixed metallic and molecular character. Binding processes such as this are characteristic of chemisorption and this result is consistent with both experimental and DFT results that alkylamines bind to Cu surfaces via nitrogen doublets<sup>30,66</sup>.

**Figure 7B** shows that HOMO-1 moves to a lower energy level by about 1.3 eV upon adsorption. The remaining orbitals are less involved in bond formation. These orbitals are more localized and have negligible overlap with the Cu *d* bands or they do not shift much in energy level, retaining mostly their molecular character. The LUMO is not involved in adsorption and remains delocalized beyond the Fermi level around 4.0 eV in both the binding and non-interacting systems, which is also an indication of a covalent Cu-N bond. We observe a similar PDOS change after binding for EDA on Cu(111), but with a smaller difference in the energy levels of the occupied orbitals. The overlap of the bound nitrogen *p*-bands with the substrate Cu *d*-bands occurs at a similar energy level, revealing a similar Cu-N

covalent bond, as well as similar charge-transfer on both Cu(100) and Cu(111).

As we noted for **Figure 3**, the binding energy of EDA on Cu(100) increases with decreasing coverage, and similar behavior is also observed for the short-range interaction between EDA and the Cu substrate. From investigations of the electronic structure, it is possible the bond strength of EDA on Cu(100) is affected by both charge transferred during EDA adsorption and the bond length. To quantify the electrostatic effect, the charge on Cu and the NH<sub>2</sub> groups in EDA adsorption is determined using Bader charge analysis and results are summarized in **Table S4**.<sup>67–70</sup> We see from all cases that NH<sub>2</sub> groups are negatively charged while the top Cu layer in the slab is positively charged, in agreement with the PDOS analysis. Additionally, the amount of charge on the top Cu layer and NH<sub>2</sub> group is similar across different coverages of EDA. N atoms are chemisorbed at atop sites with overall charge transfer from the Cu slabs to the molecules.

### EDA in Preventing Cu Surfaces against Oxidation

It has been observed experimentally that Cu(100) is oxidized faster than Cu(111) in the presence of EDA, which facilitates the anisotropic growth of Cu nanowires.<sup>46</sup> To probe the effects of EDA in inhibiting the oxidation of the Cu surfaces, we calculated the energy barrier for a water molecule to diffuse through an EDA adlayer to approach the Cu slabs. Based on *ab initio* thermodynamics (**Figure 6**), we selected 0.25 ML coverage – the highest coverage for the EDA adlayers on both Cu surfaces, as the capability of EDA to protect the surfaces is the highest at the highest coverages.

We consider the situation in which one water molecule initially resides above the EDA adlayer and is in a minimum near the surface in the final state. The initial and final states were obtained by placing a water molecule above and below the EDA layers at different sites and performing structural optimization. We used the Climbing Image Nudged Elastic Band (CI-NEB) method to find the minimum-energy pathway (MEP) between the initial and final states, including the transition state.<sup>71</sup> Both transition states on Cu(100) and Cu(111) were confirmed with one imaginary frequency. Energies from the CI-NEB calculations can be found in **Table S5**. We obtained an energy break-down for all images on the MEPs into EDA-Cu interactions, H<sub>2</sub>O-Cu interactions, and H<sub>2</sub>O-EDA interactions (cf., Equations S1-S3) and the results are summarized in **Table S6**.

On both Cu(100) and Cu(111), the water molecule resides above the EDA layer in the initial state (see screenshots for image 0 in **Figures 8A** and **8B**), while the position of the water molecule varies in the final states on the two different surfaces. From the insets in **Figure 8A**, we see water approaches Cu(111) by changing places with an adsorbed EDA, so water resides close to Cu(111) and EDA is physisorbed above the layer (image 7 in **Figure 8A**). On Cu(100), the water molecule resides close to the surface, but within the EDA layer in the optimal final state (image 7 in **Figure 8B**). The final state is less stable than the initial state on Cu(111), while the final state is more stable on Cu(100). Also, the energy barrier for water to access the final state is substantially lower on Cu(100) (0.22 eV) than on Cu(111) (0.96 eV). The high barrier on Cu(111) and the low barrier on Cu(100)

both indicate Cu(111) provides good protection against oxidation, while Cu(100) is poorly protected. These observations are consistent with experiment.

Most of the differences between the two surfaces can be attributed to the higher density of the EDA layer on Cu(111) than on Cu(100). Even though the EDA coverage is the same on both surfaces, the higher density of surface atoms on Cu(111) leads to a denser EDA adlayer. The higher EDA density on Cu(111) can be seen by comparing **Figures 2A** and **4A**.

The effects of the higher EDA density on Cu(111) can be seen in **Table S6**, where the most distinguishing energy is the EDA-water interaction. On Cu(100), the EDA-water interaction increases continually as water transits from the initial state to the final state, where the total energy is lower than in the initial state. However, the EDA-water interaction goes through a minimum and becomes repulsive at the transition state on Cu(111) before increasing to a maximum at the final state. The repulsion at the transition state, the higher energy at the final state relative to the initial state, and the fact that water cannot reside close to the surface without displacing EDA on Cu(111) all reflect denser EDA packing. Because of the denser EDA packing, Cu(111) is better protected from oxidation than Cu(100).

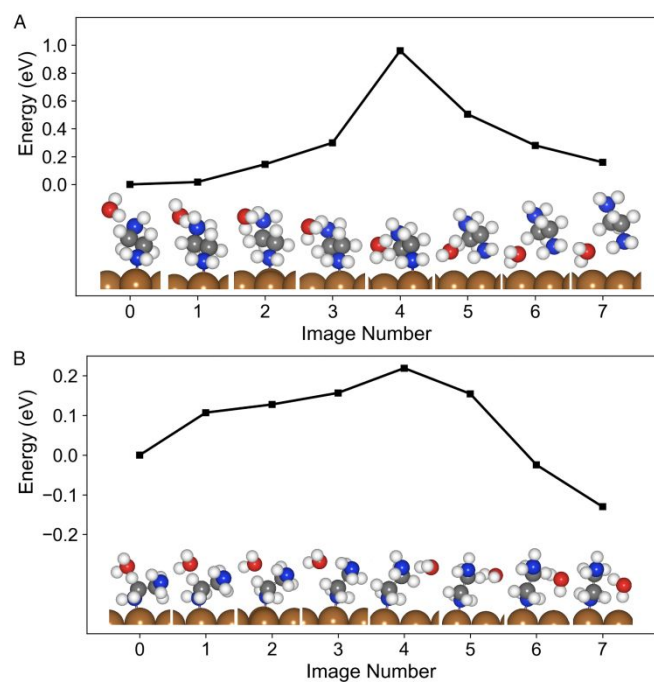


**Figure 8.** Minimum-energy pathways for a water molecule to transit through EDA with 0.25 ML coverage on (A) Cu(111) and (B) Cu(100). Energies are relative to the energy of image 0. The insets show snapshots of the EDA and water for all states (Image Number) along the pathways. (Brown: Cu, Blue: N, Gray: C, and White: H).

## Conclusions

In summary, we investigated the adsorption of EDA on both Cu(100) and Cu(111). We find N atoms prefer to reside atop Cu surface atoms. Both long-range vdW and short-range, direct bonding interactions play important roles in EDA binding. The Cu-N bond strength decreases with increasing EDA surface coverage. Structural distortions of EDA also affect the binding, especially at higher coverages.

One goal of this study was to validate the hypothesis that preferential binding of EDA on Cu(100) promotes nanowire growth. We note the binding energy of EDA on Cu(100) is generally higher than that on Cu(111) with a difference larger than 0.1 eV. This confirms the preference of EDA binding for Cu(100) and agrees well with synthetic results. However, the binding of EDA to Cu(100) is not strong enough to lower its surface energy below that of Cu(111), so there is no thermodynamic driving force for {100} facet formation.

We investigated the selective oxidation of EDA-covered Cu surfaces by probing the energy barrier for a water molecule to diffuse through the EDA adlayers with the highest surface coverages. We found a substantially lower activation barrier on Cu(100), which agrees well with the experimental observation of faster oxidation on Cu(100). We attributed the higher energy barrier for water diffusion through the EDA layer on Cu(111) to denser EDA packing on Cu(111). The capability of first-principles DFT studies to quantify successful attributes of EDA as a capping molecule implies the potential of DFT to aid in identifying promising capping agents for nanocrystal shape design.

## Conflicts of interest

There are no conflicts to declare.

## Acknowledgements

This work was supported by the Department of Energy, Office of Basic Energy Sciences, Materials Science Division, DE-FG02-07ER46414. Z.C. acknowledges training provided by the Computational Materials Education and Training (CoMET) NSF Research Traineeship (DGE-1449785).

## References

- 1 P. Christopher and S. Linic, *J. Am. Chem. Soc.*, 2008, **130**, 11264–11265.
- 2 W. D. Michalak, J. M. Krier, K. Komvopoulos and G. A. Somorjai, *J. Phys. Chem. C*, 2013, **117**, 1809–1817.
- 3 F. S. Roberts, K. P. Kuhl and A. Nilsson, *Angew. Chemie Int. Ed.*, 2015, **54**, 5179–5182.
- 4 B. Xiao, Z. Niu, Y.-G. Wang, W. Jia, J. Shang, L. Zhang, D. Wang, Y. Fu, J. Zeng and W. He, *J. Am. Chem. Soc.*, 2015, **137**, 3791–3794.
- 5 G. Li, H. Kobayashi, S. Dekura, R. Ikeda, Y. Kubota, K. Kato, M. Takata, T. Yamamoto, S. Matsumura and H. Kitagawa, *J. Am. Chem. Soc.*, 2014, **136**, 10222–10225.
- 6 P. Jena, *J. Phys. Chem. Lett.*, 2011, **2**, 206–211.

- 7 N. N. Jason, W. Shen and W. Cheng, *ACS Appl. Mater. Interfaces*, 2015, **7**, 16760–16766.
- 8 B. J. Wiley, Z. Wang, J. Wei, Y. Yin, D. H. Cobden and Y. Xia, *Nano Lett.*, 2006, **6**, 2273–2278.
- 9 L. Hu, H. S. Kim, J.-Y. Lee, P. Peumans and Y. Cui, *ACS Nano*, 2010, **4**, 2955–2963.
- 10 A. R. Rathmell and B. J. Wiley, *Adv. Mater.*, 2011, **23**, 4798–4803.
- 11 J. Zhu, X. Xu, J. Liu, Y. Zheng and S. Hou, *RSC Adv.*, 2015, **5**, 74126–74131.
- 12 Z. Zhong, H. Lee, D. Kang, S. Kwon, Y.-M. Choi, I. Kim, K.-Y. Kim, Y. Lee, K. Woo and J. Moon, *ACS Nano*, 2016, **10**, 7847–7854.
- 13 S. Chen, H. a. Gasteiger, K. Hayakawa, T. Tada and Y. Shao-Horn, *J. Electrochem. Soc.*, 2010, **157**, A82–A97.
- 14 H. You, S. Yang, B. Ding and H. Yang, *Chem. Soc. Rev.*, 2013, **42**, 2880–2904.
- 15 T. H. Yang, Y. Shi, A. Janssen and Y. Xia, *Angew. Chemie - Int. Ed.*, 2020, **59**, 15378–15401.
- 16 J. Zeng, X. Xia, M. Rycenga, P. Henneghan, Q. Li and Y. Xia, *Angew. Chemie - Int. Ed.*, 2011, **50**, 244–249.
- 17 B. Wiley, Y. Sun, B. Mayers and Y. Xia, *Chem. Eur. J.*, 2005, **11**, 454–463.
- 18 B. Wiley, Y. Sun and Y. Xia, *Acc. Chem. Res.*, 2007, **40**, 1067–1076.
- 19 X. Xia, J. Zeng, L. K. Oetjen, Q. Li and Y. Xia, *J. Am. Chem. Soc.*, 2012, **134**, 1793–1801.
- 20 A. R. Rathmell, S. M. Bergin, Y. L. Hua, Z. Y. Li and B. J. Wiley, *Adv. Mater.*, 2010, **22**, 3558–3563.
- 21 M. Jin, G. He, H. Zhang, J. Zeng, Z. Xie and Y. Xia, *Angew. Chemie - Int. Ed.*, 2011, **50**, 10560–10564.
- 22 D. V. R. Kumar, I. Kim, Z. Zhong, K. Kim, D. Lee and J. Moon, *Phys. Chem. Chem. Phys.*, 2014, **16**, 22107–22115.
- 23 M. J. Kim, S. Alvarez, T. Yan, V. Tadepalli, K. A. Fichthorn and B. J. Wiley, *Chem. Mater.*, 2018, **30**, 2809–2818.
- 24 S. Ye, I. E. Stewart, Z. Chen, B. Li, A. R. Rathmell and B. J. Wiley, *Acc. Chem. Res.*, 2016, **49**, 442–451.
- 25 Y. Xia, Y. Xiong, B. Lim and S. E. Skrabalak, *Angew. Chemie Int. Ed.*, 2009, **48**, 60–103.
- 26 Y. Xia, X. Xia and H.-C. C. Peng, *J. Am. Chem. Soc.*, 2015, **137**, 7947–7966.
- 27 Y. Xia, K. D. Gilroy, H. Peng and X. Xia, *Angew. Chem. Int. Ed.*, 2017, **56**, 60–95.
- 28 Y. Zhou, W. A. Saidi and K. A. Fichthorn, *J. Phys. Chem. C*, 2013, **117**, 11444–11448.
- 29 W. A. Al-Saidi, H. Feng and K. A. Fichthorn, *Nano Lett.*, 2012, **12**, 997–1001.
- 30 S.-H. Liu, T. Balankura and K. A. Fichthorn, *Phys. Chem. Chem. Phys.*, 2016, **18**, 32753–32761.
- 31 W. A. Saidi, H. Feng and K. A. Fichthorn, *J. Phys. Chem. C*, 2013, **117**, 1163–1171.
- 32 D. S. Kilin, O. V. Prezhdo and Y. Xia, *Chem. Phys. Lett.*, 2008, **458**, 113–116.
- 33 L. Zhou, Y. Tan, J. Wang, W. Xu, Y. Yuan, W. Cai, S. Zhu and J. Zhu, *Nat. Photonics*, 2016, **10**, 393–398.
- 34 J. Y. Ye, G. A. Attard, A. Brew, Z. Y. Zhou, S. G. Sun, D. J. Morgan and D. J. Willock, *J. Phys. Chem. C*, 2016, **120**, 7532–7542.
- 35 N. Almora-Barrios, G. Novell-Leruth, P. Whiting, L. M. Liz-Marzán and N. López, *Nano Lett.*, 2014, **14**, 871–875.
- 36 J. M. Gisbert-González, J. M. Feliu, A. Ferre-Vilaplana and E. Herrero, *J. Phys. Chem. C*, 2018, **122**, 19004–19014.
- 37 X. Qi, T. Balankura, Y. Zhou and K. A. Fichthorn, *Nano Lett.*, 2015, **15**, 7711–7717.
- 38 T. Balankura, X. Qi, Y. Zhou and K. A. Fichthorn, *J. Chem. Phys.*, 2016, **145**, 144106.
- 39 T. Balankura, T. Yan, O. Jahanmahin, J. Narukatpichai, A. Ng and K. A. Fichthorn, *Nanoscale Adv.*, 2020, **2**, 2265–2270.
- 40 X. Qi, Y. Zhou and K. A. Fichthorn, *J. Chem. Phys.*, 2016, **145**, 194108.
- 41 X. Qi and K. A. Fichthorn, *Nanoscale*, 2017, **9**, 15635–15642.
- 42 Z. Chen, T. Balankura, K. A. Fichthorn and R. M. Rioux, *ACS Nano*, 2019, **13**, 1849–1860.
- 43 K. A. Fichthorn and Z. Chen, *J. Vac. Sci. Technol. A*, 2020, **38**, 023210.
- 44 M. J. Kim, S. Alvarez, Z. Chen, K. A. Fichthorn and B. J. Wiley, *J. Am. Chem. Soc.*, 2018, **140**, 14740–14746.
- 45 M. J. Kim, M. A. Cruz, Z. Chen, H. Xu, M. Brown, K. A. Fichthorn and B. J. Wiley, *Chem. Mater.*, 2021, **33**, 881–891.
- 46 M. J. Kim, P. F. Flowers, I. E. Stewart, S. Ye, S. Baek, J. J. Kim and B. J. Wiley, *J. Am. Chem. Soc.*, 2017, **139**, 277–284.
- 47 K. A. Fichthorn, Z. Z. Chen, Z. Z. Chen, R. M. Rioux, M. J. Kim and B. J. Wiley, *Langmuir*, 2021, **37**, 4419–4431.
- 48 V. Mastronardi, G. Udayan, G. Cibecchini, R. Brescia, K. A. Fichthorn, P. P. Pompa and M. Moglianetti, *ACS Appl. Mater. Interfaces*, 2020, **12**, 49935–49944.
- 49 T. Balankura, X. Qi and K. A. Fichthorn, *J. Phys. Chem. C*, 2018, **122**, 14566–14573.
- 50 S. H. Liu and K. A. Fichthorn, *J. Phys. Chem. C*, 2017, **121**, 22531–22541.
- 51 X. Qi, T. Balankura and K. A. Fichthorn, *J. Phys. Chem. C*, 2018, **122**, 18785–18794.
- 52 K. A. Fichthorn, *Mol. Simul.*, 2014, **40**, 134–140.
- 53 G. Kresse and J. Hafner, *Phys. Rev. B*, 1993, **47**, 558–561.
- 54 G. Kresse and J. Hafner, *Phys. Rev. B*, 1994, **49**, 14251–14269.
- 55 G. Kresse and J. Furthmüller, *Phys. Rev. B*, 1996, **54**, 11169–11186.
- 56 P. E. Blöchl, *Phys. Rev. B*, 1994, **50**, 17953–17979.
- 57 G. Kresse and D. Joubert, *Phys. Rev. B*, 1999, **59**, 1758–1775.
- 58 J. P. Perdew, K. Burke and M. Ernzerhof, *Phys. Rev. Lett.*, 1996, **77**, 3865–3868.
- 59 M. Methfessel and A. T. Paxton, *Phys. Rev. B*, 1989, **40**, 3616–3621.
- 60 S. Grimme, *J. Comput. Chem.*, 2006, **27**, 1787–1799.
- 61 V. G. Ruiz, W. Liu, E. Zojer, M. Scheffler and A. Tkatchenko, *Phys. Rev. Lett.*, 2012, **108**, 146103.
- 62 K. Hermann, *Crystallography and Surface Structure: An Introduction for Surface Scientists and Nanoscientists*, Wiley-VCH, 2011.
- 63 P. Song, C. S. S. Sangeeth, D. Thompson, W. Du, K. P. Loh

- and C. A. Nijhuis, *Adv. Mater.*, 2016, **28**, 631–639.
- 64 R. C. Hoft, M. J. Ford, A. M. McDonagh and M. B. Cortie, *J. Phys. Chem. C*, 2007, **111**, 13886–13891.
- 65 K. Momma and F. Izumi, *J. Appl. Crystallogr.*, 2011, **44**, 1272–1276.
- 66 A. Glaria, J. Cure, K. Piettre, Y. Coppel, C. O. Turrin, B. Chaudret and P. Fau, *Chem. - A Eur. J.*, 2015, **21**, 1169–1178.
- 67 G. Henkelman, A. Arnaldsson and H. Jónsson, *Comput. Mater. Sci.*, 2006, **36**, 354–360.
- 68 E. Sanville, S. D. Kenny, R. Smith and G. Henkelman, *J. Comput. Chem.*, 2007, **28**, 899–908.
- 69 W. Tang, E. Sanville and G. Henkelman, *J. Phys. Condens. Matter*, 2009, **21**, 84204.
- 70 M. Yu and D. R. Trinkle, *J. Chem. Phys.*, 2011, **134**, 64111.
- 71 G. Henkelman, B. P. Uberuaga and H. Jónsson, *J. Chem. Phys.*, 2000, **113**, 9901–9904.